Journal Pre-proofs

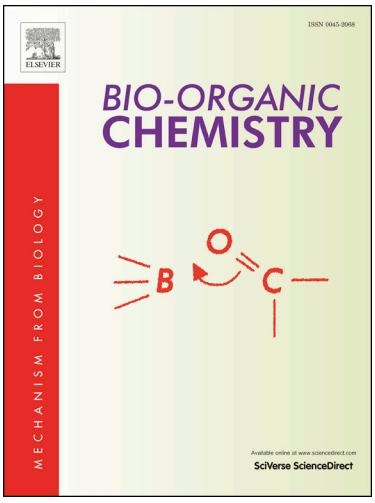

New quinoline-2-one/pyrazole Derivatives; Design, Synthesis, Molecular Docking, Anti-apoptotic Evaluation, and Caspase-3 Inhibition Assay

Ashraf A. Aly, Samia M. Sayed, El-Shimaa M. N. Abdelhafez, Sara Mohamed Naguib Abdelhafez, Walaa Yehia Abdelzaher, Mohamed A. Raslan, Amira E. Ahmed, Khaled Thabet, Ahmed A. M. El-Reedy, Alan B. Brown, Stefan Bräse

PII: S0045-2068(19)30834-X
DOI: https://doi.org/10.1016/j.bioorg.2019.103348
Reference: YBIOO 103348

To appear in: *Bioorganic Chemistry*

Received Date: 22 May 2019
Revised Date: 13 September 2019
Accepted Date: 5 October 2019

Please cite this article as: A.A. Aly, S.M. Sayed, E-S. M. N. Abdelhafez, S. Mohamed Naguib Abdelhafez, W. Yehia Abdelzaher, M.A. Raslan, A.E. Ahmed, K. Thabet, A. A. M. El-Reedy, A.B. Brown, S. Bräse, New quinoline-2-one/pyrazole Derivatives; Design, Synthesis, Molecular Docking, Anti-apoptotic Evaluation, and Caspase-3 Inhibition Assay, *Bioorganic Chemistry* (2019), doi: https://doi.org/10.1016/j.bioorg.2019.103348

New quinoline-2-one/pyrazole Derivatives; Design, Synthesis, Molecular Docking, Anti-apoptotic Evaluation, and Caspase-3 Inhibition Assay

Ashraf A. Aly,[a]* Samia M. Sayed,[b] El-Shimaa M. N. Abdelhafez,[c] Sara Mohamed Naguib Abdelhafez,[d] Walaa Yehia Abdelzaher,[e] Mohamed A. Raslan,[b] Amira E. Ahmed,[b] Khaled Thabet,[f] Ahmed A. M. El-Reedy,[g] Alan B. Brown,[h] and Stefan Bräse[i,j]

[a] Department of Organic Chemistry, Faculty of Science, Minia University, 61519-ElMinia, Egypt, [b] Aswan University, Faculty of Science, Chemistry Department, 81529 Aswan, Egypt, [c] Department of Medicinal Chemistry, Faculty of Pharmacy, 61519-El-Minia University, Egypt, [d] Department of Histology, Faculty of Medicine, Minia University, 61519-ElMinia, Egypt, [e] Department of Pharmacology, Faculty of Medicine, Minia University, 61519-El-Minia Egypt, [f] Department of Biochemistry, Faculty of Pharmacy, Minia University, 61519 El-Minia, Egypt, [g] Basic and Applied Science Department, Faculty of Oral and Dental Medicine, Nahda University, Beni Suef, Egypt, [h] Chemistry Program, Florida Institute of Technology, Melbourne, FL 32901, USA, [i] Institute of Organic Chemistry, Karlsruhe Institute of Technology, 76131 Karlsruhe, Germany, [j] Institute of Toxicology and Genetics, Karlsruhe Institute of Technology, Eggenstein-Leopoldshafen, Germany.

Corresponding authors: Prof Ashraf A Aly; e-mail: ashrafaly63@yahoo.com and ashraf.shehata@mu.edu.eg

Prof Ashraf A. Aly, Prof of Organic Chemistry, Department of Organic Chemistry, Faculty of Science, Minia University, 61519-El-Minia, Egypt, e-mail: e-mail: ashrafaly63@yahoo.com and ashraf.shehata@mu.edu.eg

Prof Samia M. Sayed: Aswan University, Faculty of Science, Chemistry Department, 81529 Aswan, Egypt; e-mail: aomabdo@yahoo.com

Dr El-Shimaa M. N. Abdelhafez: Department of Medicinal Chemistry, Faculty of Pharmacy, 61519-El-Minia University, Egypt; e-mail: shimaanaguib_80@mu.edu.eg

Dr Sara Mohamed Naguib Abdelhafez: Department of Histology, Faculty of Medicine, Minia University, 61519-El-Minia, Egypt; e-mail: *sara_histology@yahoo.com*

Dr Walaa Yehia Abdelzaher: Department of Pharmacology, Faculty of Medicine, Minia University, 61519-El-Minia Egypt; e-mail: walaayehia22@yahoo.com

Prof Mohamed A. Raslan: Aswan University, Faculty of Science, Chemistry Department, 81529 Aswan, Egypt; e-mail: raslanma47@yahoo.com

Mrs. Amira E. Ahmed, M.Sc. Student, Aswan University, Faculty of Science, Chemistry Department, 81529 Aswan, Egypt; e-mail: amiraessam394@yahoo.com

Dr Khaled Thabet: Department of Biochemistry, Faculty of Pharmacy, Minia University, 61519 El-Minia, Egypt; e-mail: khaled_thabet@minia.edu.eg

Dr Ahmed A. M. El-Reedy: Basic and Applied Science Department, Faculty of Oral and Dental Medicine, Nahda University, Beni Suef, Egypt; e-mail: ahmed.reedy78@gmail.com

Prof Alan B. Brown, Chemistry Program, Florida Institute of Technology, Melbourne, FL 32901, USA, e-mail: abrown@fit.edu.

Prof Stefan Bräse, Prof of Organic Chemistry, Institute of Organic Chemistry, Karlsruhe Institute of Technology, 76131 Karlsruhe, German, e-mail: stefan.braese@kit.edu

Abstract

We report the synthesis of new quinoline-2-one/pyrazole hybrids and their antiapoptotic activity. This effect was studied in sight of decreasing tissue damage induced by I/R in colon of rats using *N*-acetylcysteine (NAC) as anti-apoptotic reference. Compounds **6a**, **6c** and **6f** showed significant improvement for oxidative stress parameters MDA, SOD, GSH and NOx in comparison with model group and greater than the reference NAC (*N*-acetylcysteine), whereas compounds **6d** and **6e** exhibited weaker antioxidant activity when compared with the reference NAC. Moreover, compounds **6a, 6c** and **6f** showed significant decrease in inflammatory mediators TNFα and CRB greater than NAC when compared to model group exhibited significant decrease in comparable to NAC especially compound **6c** whose found CRB conc 1.90 (mg/dL) in comparison to NAC of conc 2.13 mg/dL. Additionally, colonic histopathological investigation was performed to all targeted compounds that indicates H&E sections of compounds **6a** and **6f** revealed apparent normal colonic cells while compound **6e** showed dilated blood vessels with more apoptotic cells if compared with NAC. Caspase-3 inhibition assay revealed that compounds **6a**, **6b** and **6d** weaken caspase-3 expression to an extent higher than NAC (1.063, 0.430, 0.731 and 1.115, respectively). Docking studies with caspase-3 revealed that most of the tested compounds show good binding with the enzyme especially for compound **6d** make several interactions better than that of the reference NAC.

Key words: Anti-apoptotic Quinoline; Pyrazole; Caspase-3, NAC, Histopathology, Antioxidant, Colon, Docking.

1. Introduction

Apoptosis is an essential biological process in cells during animal development tissue [1] homeostasis [2] and immune responses [3]. However, it is essential in normal physiological

events in healthy organism, imbalance probably occurs in some cases between apoptotic and anti apoptotic mediators leading to some diseases which is attributed to overexpression or inhibition of apoptotic mediators. it can be abrogated in pathological states as in cancer [4] and autoimmunity [5], or exacerbated as in stroke [6], neurodegeneration [7], retinal cell death [8], myocardial and liver ischemia [9,10], inflammatory diseases such as sepsis [11], osteoarthritis (OA) [12], rheumatoid arthritis [13], and asthma [14].

One of these mediators, is caspases family which consists of 14 mammalian caspases. Among them, apoptotic caspase -2, -3, -6, -7, -8, 9-, and -10. They use a nucleophilic cysteine in its active site to cleave aspartic acid peptide bonds within proteins. They have been considered hot targets of compound design for many years ago, because dysregulation of caspase activity leads to many severe diseases. We focused our studying on the executioner caspase-3, as it was found to be generally more promiscuous than caspase-7 and appears to be the major executioner caspase during the demolition phase of apoptosis. So caspase-3 plays a key executioner role and its inhibition can drastically prevent apoptosis in *vitro* and in *vivo* as well [15].

Currently, acute mesenteric ischemia is a life-threatening clinical complication results during extravascular events like strangulated hernia, volvulus, intussusceptions, and adhesive obstruction. Ischemia/reperfusion (I/R) injury is restoration of blood supply to organs after an ischemic period leading to parenchymal damage [16]. I/R injury elevates mortality rates to 60–80% incidence. Gut barrier disruption along with distribution of endotoxin into the circulation are revealed while (I/R), leading to severe systemic inflammation and eventually and exacerbate apoptosis leading to organ failure [17,18].

Several publications have appeared in recent years documenting quinoline and pyrazole scaffold are widely found in diverse pharmacologically active substances working as antiapoptotic agents.

Rebamipide I is an antioxidative agent which attenuates the increase in apoptosis in the intestinal mucosa after ischaemia-reperfusion but was not completely abolished [19].

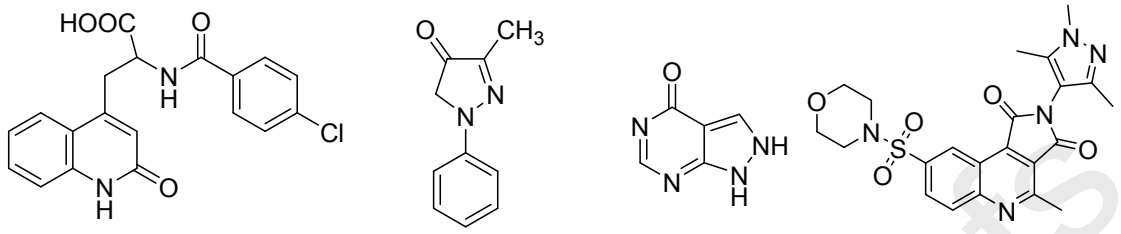

Figure 1. Structures of some antioxidant agents used against ischemia-reperfusion injury in the intestine

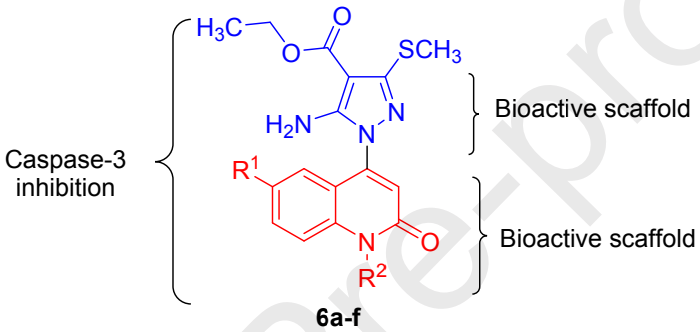

Figure 2. Design of the target compounds **6a-f**

It was demonstrated that Edaravone **II** [20] as well as alluprinol **III** [21] a pyrazole containing compounds, have potential free radical scavenging and antioxidant activities in a model of intestinal I/R injury that can prevent the aggravation of the small intestinal mucosal damage occurring during reperfusion. It's interestingly when gathering both moieties as in compound **IV**, it exhibited anti-apoptosis activity through inhibition of caspase-3 with an IC_{50} = 4 nM [22].

Because of the emergence of acute mesenteric ischemia and its on-going impact on global health system, there has been a growing interest for development of novel anti-apoptotic agents in order to combat this disorder. As a result, hybrids of quinoline and pyrazole moieties had been considered as interesting targets for designing new anti-apoptotic agents such have the structure of compounds **6a-f** (Figure 2).

Recently, we prepared ethyl pyranoquinoline-4-carboxylates and dialkyl 2(4-oxo-1,4-dihydroquinolin-3-yl)fumarates [23]. We also reacted 4-hydroxy-2-quinolones with 2-(2-oxo-1,2-dihydroindol-3-ylidene)malononitrile in pyridine, and spiro(indoline-3,4'-pyranoquinoline)-3'-carbonitriles were obtained in good to excellent yields [24]. Moreover, we synthesized bis(4-hydroxy-2-oxo-1,2-dihydroquinolin-3-yl)succinic acid derivatives by one-pot reaction of one equivalent of aromatic amines with two equivalents of diethyl malonate in diphenyl ether and catalyzed with triethylamine [25]. Reaction of four equivalents of 4-hydroxyquinolin-2(1*H*)-ones with one equivalent of acenaphthoquinone gave 1,2-dihydroacenaphthylene)-1,1,2,2-tetrayl-tetrakis(4-hydroxyquinolin-2(1*H*)-ones) in a good to excellent yields [26]. In the view of biological and pharmaceutical activities, we reported on the design and synthesis of novel series of fused naphthofuro[3,2-*c*]quinoline-6,7,12-triones and pyrano[3,2-*c*]quinoline-6,7,8,13-tetraones as potential ERK inhibitors. The synthesized inhibitors were evaluated for their ability to inhibit ERK1/2 in an *in vitro* radioactive kinase assay [27]. Also, two series of *N*-2,3-bis(6-substituted-4-hydroxy-2-oxo-1,2-dihydroquinolin-3-yl)naphthalene-1,4-diones and substituted *N*-(methyl-/ethyl)bisquinolinone triethyl-ammonium salts were successfully synthesized. The synthesized compounds were targeted as candidates to extracellular signal-regulated kinases ERK1/2 with considerable antineoplastic activity. To further elucidate the mechanism of action of these synthesized compounds selected to investigate for their MAP Kinases pathway inhibition together with molecular docking using ATP-binding site of ERK2 [28]. Encouraged by the biological and pharmaceutical activities of 2-quinolones, we have recently reported a review article which discusses the recent synthetic approaches and the applications of this class of compounds in the synthesis of related four-membered to seven-membered heterocycles, most of them showing unique biological activities [29]. Two series of diethyl 2-[2-(substituted-

2-oxo-1,2-dihydroquinolin-4-yl)hydrazono]succinates and 1-(2-oxo-1,2-dihydroquinolin-4-yl)-1*H*-pyrazole**s** have been designed and synthesized. Seven compounds were further examined against the most sensitive cell lines, leukemia CCRF-CEM, and MOLT-4.One compound was shown high activity with IC_{50} = 1.35 uM and 2.42 uM against MOLT-4 and CCRF-CEM, respectively. Also, it showed a remarkable inhibitory activity compared to Erlotinib on the EGFR TK with IC_{50} = 247.14 nM and 208.42 nM, respectively [30].

The present work involves the synthesis of new quinolin-2-one/pyrazole hybrids **6a-f** substituted with either electron donating or withdrawing groups to study their electronic effect. In addition, screening of their anti-apoptotic activity, molecular modelling studies and caspase-3 inhibition assay have been carried out to study the plausible mechanism of action of the newly synthesized compounds.

2. Results and Discussion

2.1. Chemistry

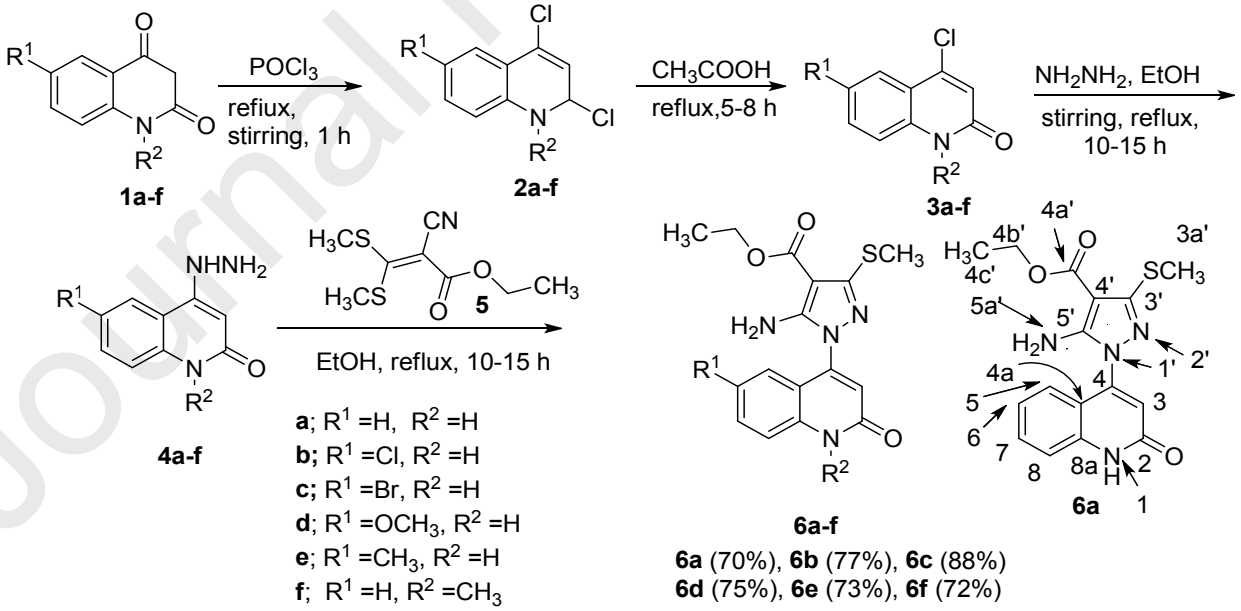

Scheme 1. Synthesis of the target compounds **6a-f**

The strategy involved the reaction of $POCl_3$ with quinoline-2,4-diones **1a-f** to give the corresponding dichlorotetrahydroquinoline **2a-f** [31-33]. Oxidation of **2a-f** gave the monochloro derivatives **3a-f**, which on heating with hydrazine hydrate yielded the quinolones **4a-f** [33] (Scheme 1). Refluxing **4a-f** with ethyl 2-cyano-3,3-bis(methylthio)propenoate (**5**) in absolute ethanol afford the target compounds **6a-f** in good yields [31]. The newly synthesized compounds were identified by 1D-NMR (^{1}H NMR, ^{13}C NMR), 2D-NMR (COSY, HSQC, HMBC) and mass spectra. As an example, NMR spectra of compound **6a** (Table 1) showed the ethyl ester signals are distinctive at δ_H 1.29 (t; H-4c') and 4.23 (q; H-4b'), and δ_C 14.46 (C-4c') and 59.07 (C-4b'). H-4b' give HMBC correlation with one of the two carbons at δ_C 162.95 and 161.65, which is assigned as C-4a'. The methylthio protons H-3a' are also distinctive, at δ_H 2.35; their attached carbon appears at δ_C 12.31. H-3a' also give HMBC correlation with a carbon at δ_C 91.69, assigned as C-4'; its upfield chemical shift is attributed to its position in a push-pull system. The broad 3H signal at δ_H 6.60 gives both H-C HSQC correlation, with a carbon at δ_C 120.25, and H-N HSQC correlation, with a nitrogen at δ_N 59.8. This proton "signal" is therefore assigned as co-resonant signals from H-3 and H-6a'. A carbon at δ_C 152.44, which gives no correlations, is assigned on chemical-shift grounds as C-5'; N-2', which is four bonds from the nearest protons, is not observed at all. The signals of the quinolinone part structure are assigned straight forwardly, and are similar to those of recently-studied quinolinones with the same substitution pattern. The signal at δ_H gives HMBC correlation with a carbon at δ_C 144.20, assigned as C-4. C-4 gives HMBC correlation with a doublet at δ_H 7.32, assigned as H-5; its attached carbon appears at δ_C 124.53. C-5 gives HMBC correlation with a "triplet" at δ_H 7.58, assigned as H-7; this is a three-bond correlation. H-7 gives HSQC correlation with its attached carbon at δ_C 131.16. The other "triplet" of the four-spin aromatic pattern, at δ_H 7.20, is assigned as H-6; its attached carbon

appears at δ_C 122.01. C-6 in turn gives HMBC correlation with the other doublet of the four-spin pattern, at δ_H 7.41; this doublet is assigned as H-6, and its attached carbon appears at δ_C 115.56. The non-protonated carbons at δ_C 139.56 and 116.52 are assigned as C-8a and C-4a respectively; their chemical shifts and correlations are consistent with these assignments. Finally, the other of the carbons at δ_C 162.95 and 161.65 is assigned, on chemical-shift grounds, as C-2.

Table 1. NMR spectroscopic data of compound **6a**

^{1}H NMR (DMSO-d_6)	**^{1}H-^{1}H COSY**		**Assignment**
12.07 (bs; 1H)	6.60		H-1
7.58 ("t", *J* = 7.6; 1H)	7.41, 7.32, 7.20		H-7
7.41 (d, *J* = 8.1; 1H)	7.85, 7.32, 7.20		H-8
7.32 (d, *J* = 8.0; 1H)	7.85, 7.41, 7.20		H-5
7.20 ("t", *J* = 7.6; 1H)	7.85, 7.40, 7.32		H-6
6.60 (s; 3H)	12.07		H-3, 6a'
4.23 (q, *J* = 7.1; 2H)	1.29		H-4b'
2.35 (s; 3H)			H-3a'
1.29 (t, *J* = 7.0; 3H)	4.23		H4c'
^{13}C NMR (DMSO-d_6)	**HSQC**	**HMBC**	**Assignment**
162.95, 161.65		4.23	C-2, 4a'
152.44			C-5'
149.94		2.35	C-3'
144.20		7.32, 6.60	C4
139.56		7.58, 7.32	C-8a
131.16	7.58	7.32	C-7
124.53	7.32	7.58	C-5
122.01	7.20	7.41	C-6
120.25	6.60		C-3
116.52		12.07, 7.41, 7.20	C-4a
115.56	7.41		C-8
112.41			C≡N
91.69		6.60	C-4'
59.07	4.23	1.29	C-4b'
14.46	1.29		C-4c'
12.31	2.35		C-3a'
^{15}N NMR(DMSO-d_6)	**HSQC**	**HMBC**	**Assignment**
181.4		6.60	N-1'
151.1	12.07		N-1
59.8	6.60		N-6a'

In case of **6d**, NMR spectroscopic data (Table 3) showed the methylthio protons H-3a' are also distinctive, at δ_H 2.37; their attached carbon appears at δ_C 12.38. H-3a' also give HMBC correlation with a carbon at δ_C 91.81, assigned as C-4'; its upfield chemical shift is attributed to

its position in a push-pull system. The broad 2H signal at δ_H 6.65 gives H-N HSQC correlation with a nitrogen at δ_N 60.7; this proton signal is assigned as H-6a'. The sharp 1H singlet at δ_H 6.58 is assigned as H-3; its attached carbon appears at δ_C 119.85.

Table 2. NMR spectroscopic data of compound **6d**

^{1}H NMR (DMSO-d_6)		**^{1}H-^{1}H COSY**	**Assignment**
11.97 (s; 1H)		6.65	H-1
7.37 (d, *J* = 9.0; 1H)		7.26	H-8
7.26 (dd, *J* = 9.0, 2.6; 1H)		7.37, 6.91	H-7
6.91 (d, *J* = 2.6; 1H)		7.26	H-5
6.65 (bs; 2H)		11.97	H-6a'
6.58 (s; 1H)			H-3
4.23 (q, *J* = 7.1; 2H)		1.29	H4B'
3.70 (s; 3H)			H-6A
2.37 (s; 3H)			H-3A'
1.29 (t, *J* = 7.1; 3H)		4.23	H-4C'
^{13}C NMR (DMSO-d_6)	**HSQC**	**HMBC**	**Assignment**
162.97		4.23	C-4a'
161.15			C-2
154.07		7.37, 7.26, 6.91, 3.70	C-6
152.46			C-5'
150.07		2.37	C-3'
143.54		7.37, 6.91, 6.58	C-4
134.19		7.37, 7.26, 6.91	C-8a
120.23	7.26	6.91	C-7
119.85	6.58		C-3
116.99, 116.93	7.37	11.97, 7.37, 6.91, 6.58	C-4a,8
106.37	6.91	7.37, 6.91, 6.58	C-5
91.81		6.65	C-4'
59.11	4.23	1.29	C-4b'
55.35	3.70		C-6a
14.44	1.29	4.23	C-4C'
12.38	2.37		C-3a'
^{15}N NMR (DMSO-d_6)	**HSQC**	**HMBC**	**Assignment**
182		6.65,658	N-1'
150.1	11.97	7.37	N-1
60.7	6.65		N-6a'

A carbon at δ_C 152.46, which gives no correlations, is assigned on chemical-shift grounds as C-5'; N-2', which is four bonds from the nearest protons, is not observed at all. The multiplicities

and coupling constants of the three protons in the benzene ring allow their immediate assignment as H-5 (δ_H 6.91), H-7 (δ_H 7.26), and H-8 (δ_H 7.37); the attached carbons appear at δ_C 106.37 (C-5), 120.23 (C-7), and either 116.99 or 116.93 (C-8). The methoxy protons H-6a are distinctive at δ_H 3.70; their attached carbon appears at δ_C 55.35. H-6a give HMBC correlation with a non-protonated carbon at δ_C 154.07, assigned as C-6; C-6 also correlates with H-5, H-7, and H-8. The remaining carbons are all non-protonated. The line at δ_C 134.19 gives HMBC correlation with H-5 and H-7 and (weakly) with H-8; the line at δ_C 143.54 correlates with H-8, H-5, and H-3. These lines are assigned as C-8a and C-4 in the order stated. The other of the lines at δ_C 116.99 and 116.93, and the line at δ_C 161.15, are assigned on chemical-shift grounds as C-4a and C-2 respectively. The ethyl ester signals are distinctive at δ_H 1.29 (t; H-4c') and 4.23 (q; H-4b'), and δ_C 14.46 (C-4c') and 59.06 (C-4b'). H-4b' give HMBC correlation with a carbon at δ_C 162.92, which is assigned as C-4a' (All carbon lines in this sample are well-separated, thus all correlations are unambiguous). Interestingly, H-4c' gives a weak HMBC correlation with a carbon at δ_C 91.63, assigned on chemical-shift grounds as C-4'; its upfield chemical shift is attributed to its position in a push-pull system. In other samples of this series, C-4' gives correlation with the methylthio protons, but in this sample it does not. In case of **6f**, the NMR spectroscopic data (Table 3) revealed the methylthio protons H-3a'at δ_H 2.34; their attached carbon appears at δ_C 12.32. H-3a' also give HMBC correlation with a carbon at δ_C 150.00, assigned as C-3'. A carbon at δ_C 152.57, which gives no correlations, is assigned on chemical-shift grounds as C-5'; N-2', which is four bonds from the nearest protons, is not observed at all. The broad 2H signal at δ_H 6.59 gives H-N HSQC correlation with nitrogen at δ_N 60.2; therefore the proton signal is assigned as H-6a' and the nitrogen is assigned as N-6a'. H-6a' also give

HMBC correlation with a nitrogen at δ_N 179.8, assigned as N-1'. N-1' gives HMBC correlation with the 1H singlet at δ_H 6.75, assigned as H-3; its attached carbon appears at δ_C 119.89.

Table 3. NMR spectroscopic data of compound **6f**

^{1}H NMR (DMSO-d_6)		**^{1}H-^{1}H COSY**	**Assignment**
7.72 (dt, J_d = 1.6, J_t = 7.6; 1H)		7.67, 7.30	H-7
7.67 (d, J = 8.1; 1H)		7.72	H-8
7.35 (dd, J = 7.9, 1.3; 1H)		7.30	H-5
7.30 (dt, J_d = 0.8, J_t = 7.3; 1H)		7.72, 7.35	H-6
6.75(s; 1H)			H-3
6.59 (bs; 2H)			H-6a'
4.23 (q, J = 7.1; 2H)		1.29	H-4b'
3.70 (s; 3H)			H-1a
2.34 (s; 1H)			H-3a'
1.29 (t, J = 7.0; 3H)		4.23	H-4c'
^{13}C NMR (DMSO-d_6)	**HSQC**	**HMBC**	**Assignment**
162.92		4.23	C-4a'
160.93		6.75, 3.70	C-2
152.57			C-5'
150.00		2.34	C3'
143.16		7.67, 7.35, 6.75	C-4
140.33		7.72, 7.35, 7.30, 3.70	C-8a
131.64	7.72	7.35, 7.30	C-7
124.99	7.35	7.72	C-5
122.25	7.30	7.67, 6.75	C-6
119.89	6.75		C-3
117.55		7.72, 7.67, 7.30, 6.75	C-4a
115.14	7.67	7.30, 3.70	C-8
91.63		1.29	C-4'
59.06	4.23	1.29	C-4b'
29.35	3.70	6.75	C-1a
14.46	1.29	4.23	C-4c'
12.32	2.34		C-3a'
^{15}N NMR (DMSO-d_6)	**HSQC**	**HMBC**	**Assignment**
179.8		6.75, 6.59	N-1'
145.9		6.75,3.70	N-1
60.2	6.59		N-6a'

H-3 also gives HMBC correlation with a nitrogen at δ_N 145.9, assigned as N-1; with non-protonated carbons at δ_C 143.16 and 117.55, assigned as C-4 and C-4a respectively; and with the *N*-methyl carbon at δ_C 29.35, assigned as C-1a. N-1 also gives HMBC correlation with the *N*-methyl protons H-1a, at δ_H 3.70; the *N*-methyl carbon and protons give HSQC correlation with

each other. H-1a also give HMBC correlation with the lactam carbonyl at δ_C 160.93, assigned as C-2; with a non-protonated carbon at δ_C 140.33, assigned as C-8a; and with a protonated carbon at δ_C 115.14, assigned as C-8. C-8 gives HSQC correlation with a 1H doublet at δ_H 7.67, assigned as H-8. C-4 gives HMBC correlation with the other end signal of the four-spin aromatic system, at δ_H 7.35; this signal appears as a double-doublet with one large *J,* and gives HSQC correlation with its attached carbon at δ_C 124.99. The proton and carbon just mentioned are assigned as H-5 and C-5 respectively.

The mechanism describes the formation of compounds **6a-f** can be explained due to nucleophilic attack of the nitrogen of the hydrazine to the active electrophilic carbon in **5** to give Zwitter ion **7** (Scheme 2). The intermediate **7** would be neutralized to give **8**, accompanied with elimination of a molecule of methylthiol to give **9** (Scheme 2). Subsequently, another nucleophilic attack of the nitrogen lone pair of the second nitrogen of hydrazine to the carbon of nitrile group would give **10** (Scheme 2). Aromatization of **9** would give compounds **6a-f** (Scheme 2).

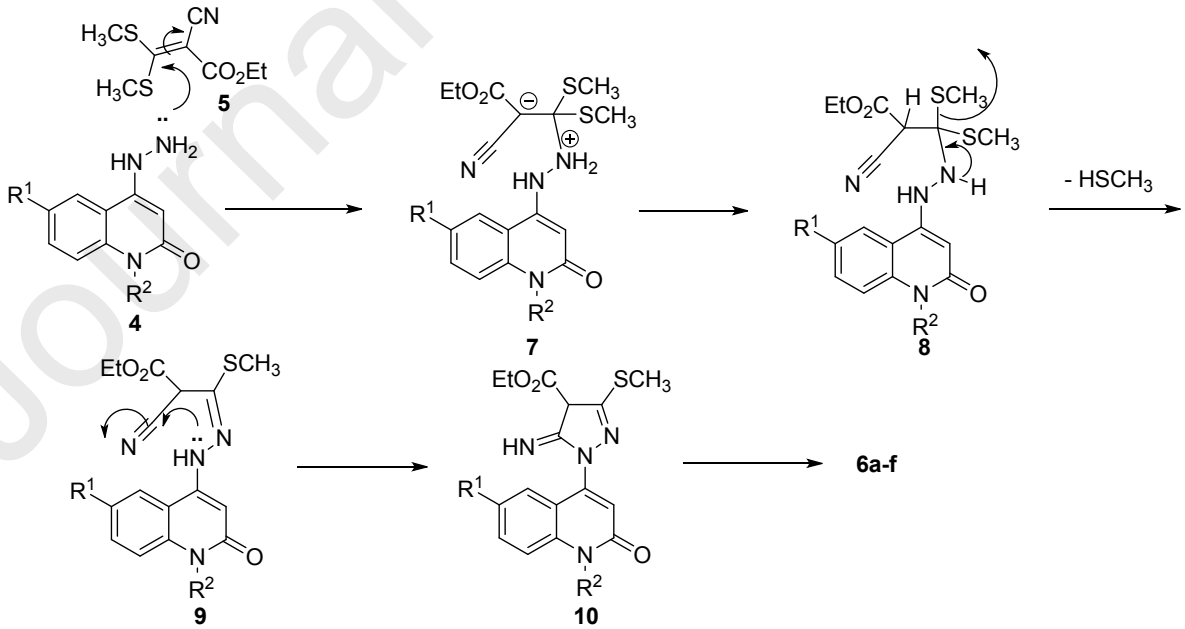

Scheme 2. Mechanism describes the formation of compounds **6a-f**

2.2. Biological Activity

2.2.1. Assay of Antioxidant biomarkers in colon (MDA, SOD, GSH, NOX)

This study showed the anti-apoptotic effect of novel compounds on decreasing tissue damage induced by I/R in colon of rats in a dose equivalent to 30 mg *N*-acetylcysteine (NAC) [34] as anti-apoptotic reference [35], when they are administrated *via* intra-peritoneal (i.p) an hour before ischemia (0.5 h) and reperfusion (0.5 h), after that the organs were cut. This was supported by biochemical, histological and morphometric studies. Different biomarker concentrations were measured in serum to detect colon injury due to ischemia/reperfusion (I/R). Some of these biomarkers are increased and others decreased indicating apoptotic effect as shown in Table 4.

Table 4. The expression of the biomarkers during apoptosis for colon

*Biomarker	Effect during apoptosis in Colon
Serum TNFα[36], MDA[37], CRB[38]	Increase
SOD[39], GSH[40], Nox[41]	Decrease

TNF = Tumor necrosis factor, **MDA** = Malondialdehyde, **SOD** = Superoxide dismutase
GSH = Glutathione, **NOx** = NADPH oxidase **CRB**= C-reactive protein (CRP)

There was a significant improvement in oxidative stress parameters MDA, SOD, GSH and NOX in comparison with model group. The results showed obviously that compounds **6a** ,**6c** and **6f** had excellent MDA inhibition effect with conc 37.89, 40.27 and 35.08 nmol/g tissue; respectively, and more than NAC (37.89 nmol/g tissue). In addition, compounds **6a**, **6c** and **6f** had SOD excellent activation effect with 149.35, 155.70 and 161.38 U/mg protein, respectively in comparison with NAC (158.61 U/mg protein) as illustrated in Table 5. Also compounds **6a** and **6f** had GSH excellent activation effect with conc 70.09 and 75.93 µmol/mg protein; respectively relative to NAC (80.25 µmol/mg protein). In addition, compounds **6a**, **6c** and **6f** had NOx excellent activation effect with conc 110.58, 112.67 and 109.73 nmol/mg protein; respectively relative to NAC (110.58 nmol/mg protein) but compound **6d** and **6e** had very weak

MDA, SOD, GSH, and NOx activation effect with significant increase in MDA with significant decrease in intestinal SOD, GSH and NOx in model group (Table 5).

Table 5. MDA, SOD, GSH and NOx concentrations in colon of I/R rats treated with compounds **6a-f** and NAC

Groups	Intestinal MDA (nmol/g tissue)	Intestinal SOD (U/mg protein)	Intestinal GSH (μmol/mg protein)	
Sham operated	30.43± 2.89	164.72±4.56	78.34±3.91	115.43±5.34
Model group	98.09±3.26a^{c}	71.34±3.60^{ac}	42.38±4.01^{ac}	69.47±4.31^{ac}
NAC	37.89±1.86b	158.61±3.27^{b}	80.25±2.59^{b}	110.58±4.89^{b}
6a	39.56±2.50^{b}	149.35±4.50^{b}	70.09±4.32^{b}	108.46±5.07^{b}
6b	65.19±3.06^{abc}	119.38±3.99^{abc}	68.45±2.91^{b}	88.54±3.46a^{bc}
6c	40.27±3.18^{b}	155.70±4.07^{b}	66.58±3.80^{b}	112.67±6.90^{b}
6d	88.09±3.71^{ac}	75.34±2.51^{ac}	44.70±3.60^{ac}	70.36±3.40^{ac}
6e	94.26±2.98^{ac}	79.61±3.49^{ac}	49.99±2.97^{ac}	73.81±4.53^{ac}
6f	35.08±3.26^{b}	161.38±4.56^{b}	75.93±4.07^{b}	109.73±5.30^{b}

2.1. Assay of inflammatory biomarkers (Serum TNFα and CRB)

The assay of inflammatory parameters (TNFα and CRP) was done in comparison with sham and NAC treated group and the results were outlined in Table 6. Compounds **6a** ,**6c** and **6f** treated groups showed significant decrease in TNFα of conc 8.4, 9.07and 8.90 pg/ml greater than NAC of conc 9.50 pg/ml when compared to model group of conc 26.67 pg/ml (table 6). Moreover, they also exhibited significant decrease in CRB comparable to NAC especially compound **6c** whose found conc 1.90 (mg/dL) in comparison to NAC of conc 2.13 mg/dL Meanwhile**,** these biomarkers were significantly increased in model, **6d** and **6e** groups in comparison with sham and NAC treated group (Table 6). It could be concluded from the previous results that unsubstituted quinoline at position 6 (compounds **6a** and **6b**) showed the highest activity and there is no great activity when substituted with either electron donating groups (CH_3, OCH_3) or withdrawing group (Cl , Br)

Table 6. TNF**α** and CRP concentrations in colon of I/R rats treated with compounds **6a-f** and **NAC**.

Groups	Serum TNFα (pg/ml)	Serum CRP (mg/dL)
Sham operated	8.34±0.75	2.00±0.18
Model group	26.67±2.60[ac]	17.45±0.93[ac]
NAC	9.50±0.57[b]	2.13±0.20[b]
6a	8.4±1.07[b]	2.40±0.17[b]
6b	15.12±1.20[abc]	12.69±0.16a[c]
6c	9.07±0.79[b]	1.90±0.14[b]
6d	23.89±1.91[ac]	15.90±0.19[ac]
6e	27.47±1.80[ac]	17.98±0.18[ac]
6f	8.90±0.61[b]	2.21±0.09[b]

Results represent the mean ± S.E (n= 5)**.** [a] Significant ($P < 0.05$) difference from sham operated group, [b] Significant ($P < 0.05$) difference from model group, [c] Significant ($P < 0.05$) difference from NAC treated group.

2.2. 2. Histopathological Investigation

Motivated by previously mentioned above results, colonic histopathological investigation was performed. the Colon sections from sham group showed normal mucosa, submucosa, musculosa and serosa. The mucosa was folded, intact and continuous, lined with simple columnar epithelial cells and had close regularly arranged crypts that appeared tubular in structure (Figure 3).

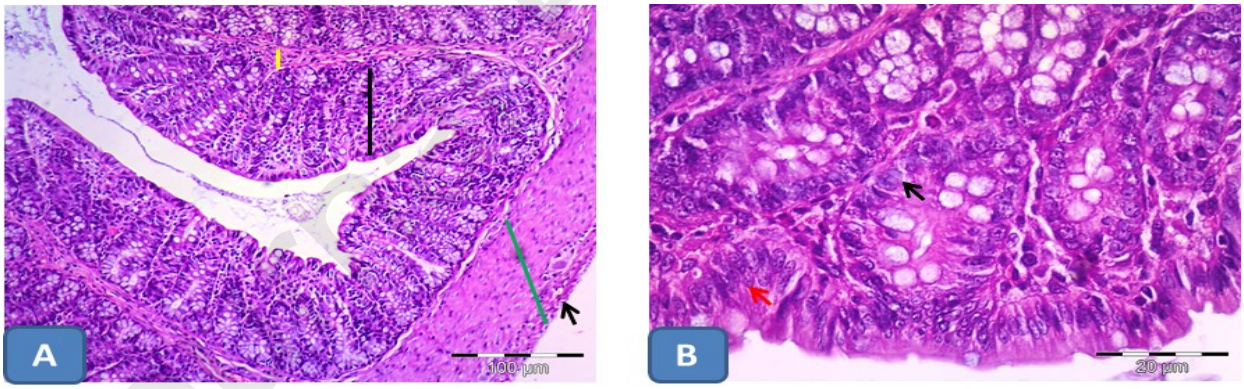

Figure 3. Photomicrographs of a section in the colon from a control rat (sham) showing A) normal mucosa (black line), submucosa (yellow line), musculosa (green arrow) and serosa (arrow). The mucosa is folded, intact and continuous. B) Notice the simple columnar epithelial cells (red arrow) lining the mucosa and has close regularly arranged tubular crypts (C). (H&E, A x100; BX 400).

While ischemic reperfusion group showed sever congestive blood vessels, distorted mucosa with absence of folding. Submucosal cellular Infiltration was clearly noticed. Detached intraluminal

debris with massive intraluminal apoptotic cells (small dense eccentric nuclei) were also observed (Figure 4). H&E sections of compound **6c** revealed apparent normal colonic cells with vesicular nuclei. Additionally, NAC as well as **6f** revealed few apoptotic cells with apparent normal colonic architecture. Compound **6a** showed dilated blood vessels with more apoptotic cells if compared with compound NAC (Figure 5).

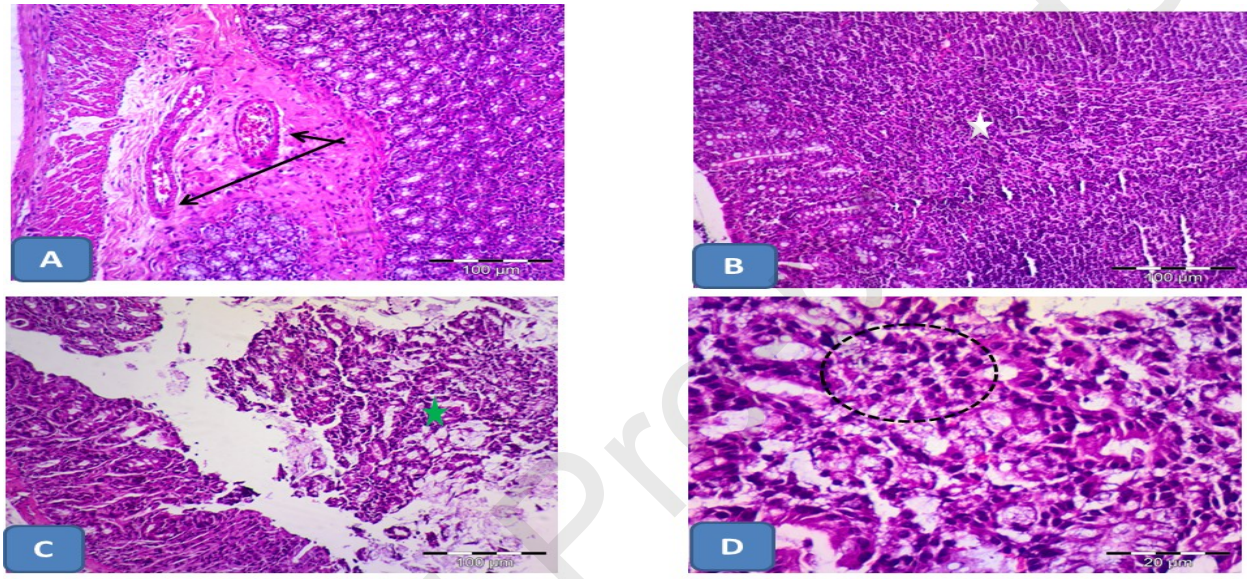

Figure 4. Photomicrographs of sections in the colon from a rat of ischemic reperfusion show congestive blood vessels (arrows). B) Distorted mucosa (star) with absence of folding. Notice the cellular Infiltration (stars) in the mucosa. C) Detached intraluminal debris (green arrow). D)Massive intraluminal apoptotic cells (small dense eccentric nuclei (circle) (H&E, A x B, C, 100; DX 400).

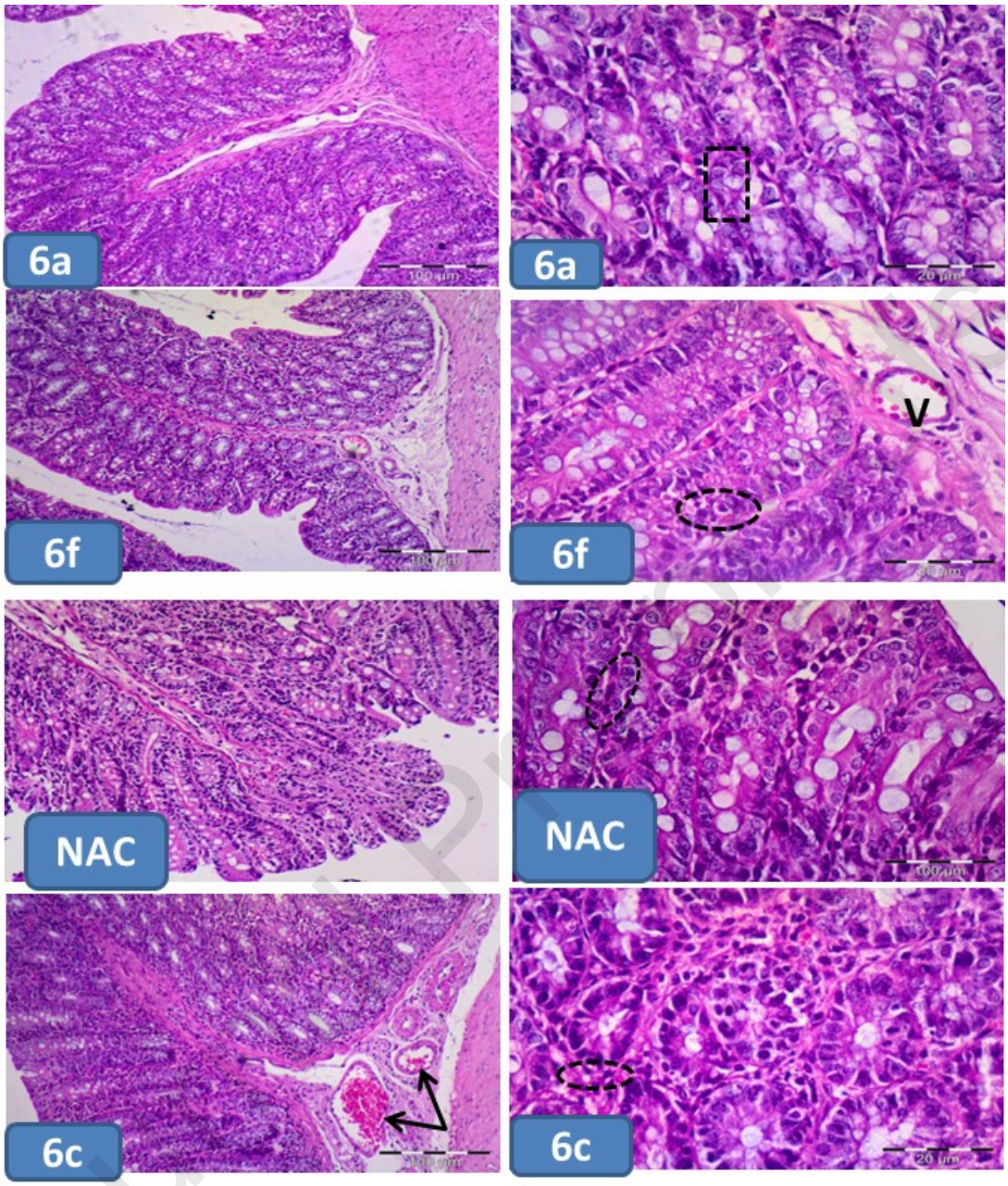

Figure 5. Photomicrographs of sections in the colon from a rat with compound **6c** showed apparent normal colonic cells with vesicular nuclei (rectangle). **NAC** and **6f** showed few apoptotic cells (circle) with apparent normal colonic architecture. Compound **6a** showed dilated blood vessels (arrows) with more apoptotic cells (circle); AX 100; BX400).

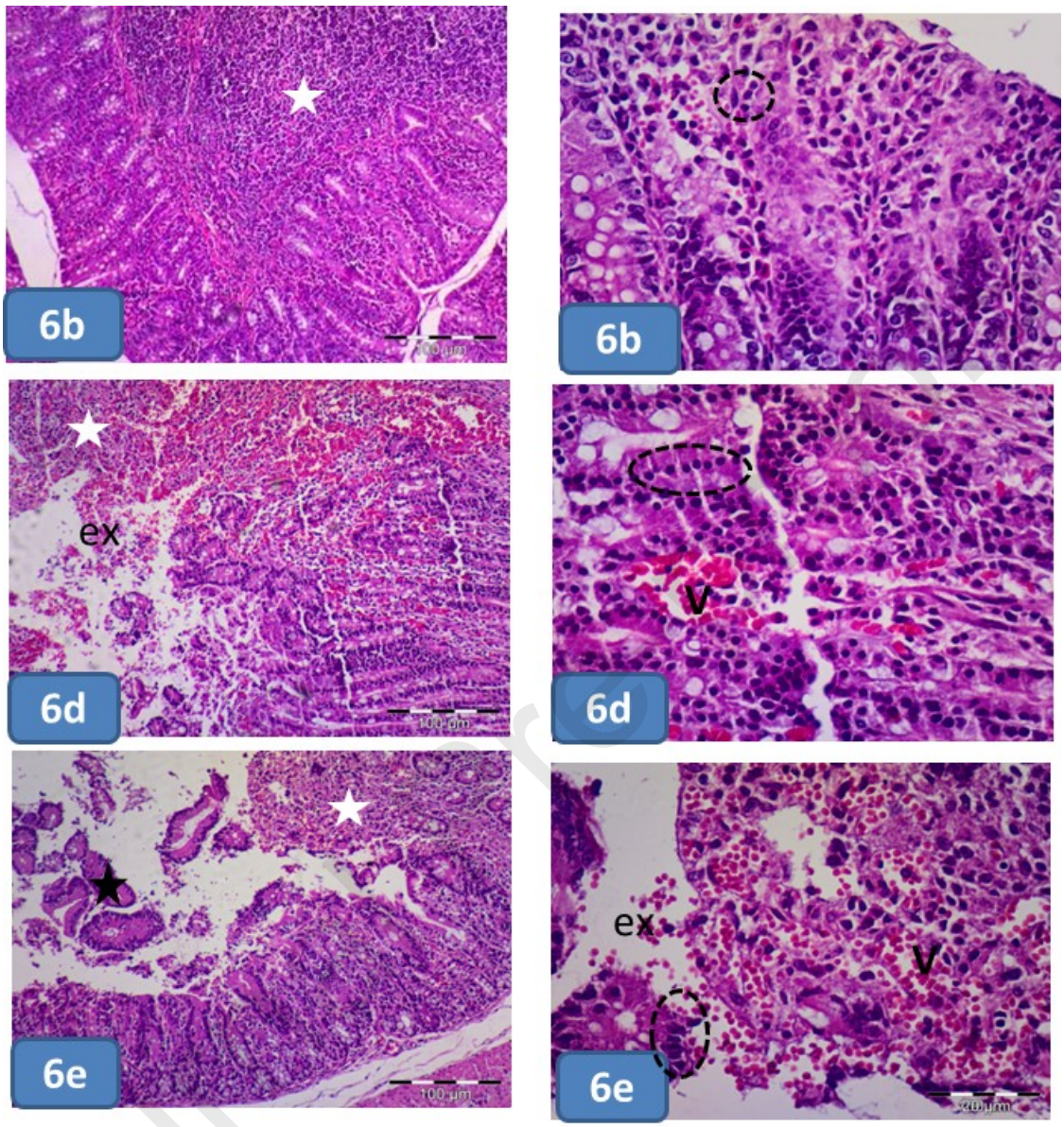

Figure 6. Photomicrographs of sections in the colon from rats together with compound **6b** which showed: inflammatory cell infiltrations (star) more numerous apoptotic cells (circle). Compound **6d** showed distorted colonic architecture with inflammatory cell infiltration (star), extravation of RBCs and congested blood vessels (V). Notice almost all colonic cells showed apoptotic cells (circle). Compound **6e** showed sever distorted colonic architecture with inflammatory cell infiltration (star), extravation of RBCs and congested blood vessels (V). Notice almost all colonic cells showing more numerous apoptotic and distorted cells (circle); AX 100; BX400).

H&E sections of compound **6b** showed inflammatory cell infiltrations and more numerous apoptotic cells than compound **6a**. Compound **6d** revealed distorted colonic architecture with

inflammatory cell infiltration. Extravation of RBCs and congested blood vessels were frequently seen. In this group almost all colonic cells showed apoptotic cells. Furthermore, compound **6e** exhibited sever distorted colonic architecture with inflammatory cell infiltration, extravation of RBCs and congested blood vessels. Almost all colonic cells showed more numerous apoptotic and distorted cells (Figure 6).

2.2.3. Morphometric results

There was significant increase in apoptotic cells in compound **6e** than compound **6d**. Also it was detected a significant increase in apoptotic cells in compound **6d** than compound **6b**. Additionally there was a significant increase in apoptotic in compound **6b** than **6a** and NAC (Figure 7).

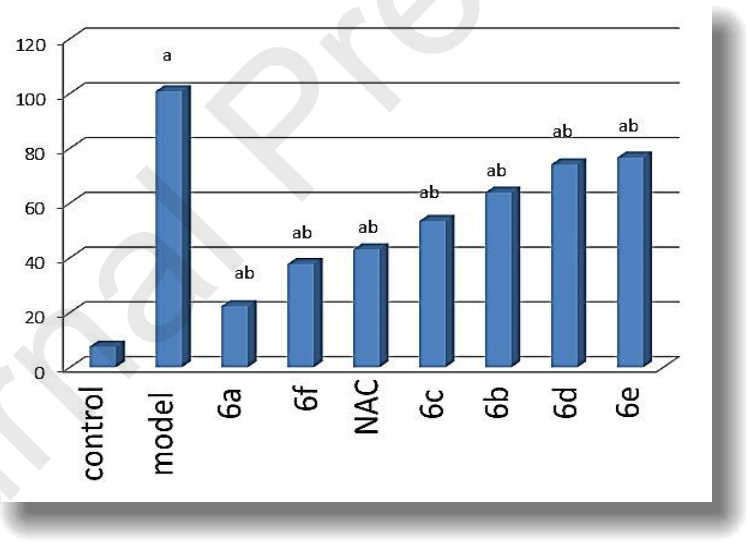

Figure 7: showing the mean number of apoptotic cells arranged ascendingly for **NAC** and **6a-f** Results represent the mean ± S.E. (n= 8). [a] Significant ($P < 0.05$) difference from group I, [b] Significant ($P < 0.05$) difference from group II.

2.3. Caspase-3 expression assay

The inhibitory activity of the newly designed derivatives was examined on caspase-3 mRNA expression level by LPS stimulated Caco-2 cells using NAC as a reference compound. Figure 8

shows the effect of the available target compounds **6a-f** on caspase-3 mRNA expression level by LPS stimulated Caco-2 cells. The significant increase in Caspase-3 mRNA expression was found in LPS stimulated cells without treatment (**A**, *P=0.018),* LPS +**6c** (**E**, *P=0.006,* caspase expression = 2.534*),* and LPS +**6e** (**G**, *P* =0.018, Fold change =2.049) in comparison to non-stimulated cells (Control). This means that bulky substituents are not favourable for caspase-3 inhibitory activity. Meanwhile treatment of LPS-stimulated cells with either *N*-acetyl cysteine (**B**, *P* =0.4, Fold change =1.115) or **6a** (**C**, *P* = 0.2, Fold change = 1.063*)* decreases the mRNA expression level of caspase-3 and returns it to the control level without any significant difference. While the significant decrease in caspase-3 mRNA expression was associated with the treatment of LPS stimulated cells with **6b** (**D**, *P* =0.02*,* Fold change =0.430) and **6d** (**F**, *P* =0.02, Fold change =0.731). Results were calculated by paired t-test using GraphPad Prism 7 Software, San Diego, CA) as shown in Table 7. The results indicate true inhibition of caspase-3.

Table 7. Fold change of caspase-3 expression **6a-f**

Fold change in Caspase-3 expression								
control	**control+LPS**	**C+LPS+ NAC**	**6a**	**6b**	**6c**	**6d**	**6e**	**6f**
1	1.988	1.115	1.063	0.430	2.534	0.731	2.049	2.376

Figure 8. Fold change of caspase-3 expression for targeted compounds **6a-e** and NAC

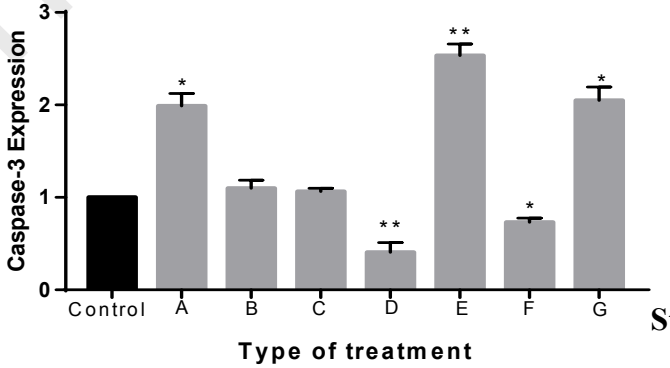

2.4. Docking Studies

Enzyme-ligand docking was carried out for all derivatives **6a-f** and NAC as a reference to predict the binding interactions between the newly synthesized quinoline/pyrazole hybrids and

caspase-3 enzyme obtained from the protein data bank (PDB:6CKZ) using Molecular Operating Environment (MOE®) version 2014.09 using NAC as reference for validation of the method. The theoretical predictions from the molecular docking study were found to be in agreement for some highly active derivatives such as **6b**, **6d** and **6a** with the experimentally observed caspase-3 inhibition activity. All derivatives were successfully docked into the active site of caspase-3 enzyme. The binding free energies from the major docked poses are listed in Table 8 and the most favourable poses of the tested compounds are shown in Figure 9. Most of the tested compounds have high binding affinity to the enzyme as the binding free energy(ΔG) values of them range from -0.6 to 3.2 Kcal/mol comparable to the reference NAC (ΔG = - 0.7 to – 2.9 Kcal/mole).

Table 8. Energy scores for the complexes formed by the tested compounds **6a-f** and the reference NAC in the active site of caspase-3 (PDB: 6CKZ)

Compound	S score	ΔG	Ligand-receptor interaction		
		(Kcal/mole)	Residue	Type	Length (Å)
NAC	-4.03	-2.9	Arg 207	H-acceptor	3.64
		-0.7	Gly122	H-acceptor	3.53
		-1.0	Arg64	H-acceptor	4.28
6a	-6.35	-2.6	Arg207	H-acceptor	3.00
		-3.2	Gly122	H-acceptor	3.19
6b	-6.45	-2.6	Arg207	H-acceptor	3.07
		-2.9	Gly122	H-acceptor	3.20
6c	-4.52	-2.6	Arg207	Pi-cation	3.61
		-1.8	Arg64	H-acceptor	3.35
		-1.2	Arg64	H-acceptor	3.51
6d	-6.65	-2.8	Arg207	H-acceptor	3.09
		-3.0	Gly122	H-acceptor	3.05
		-0.6	Trp206	H-Pi	4.41
6e	-4.56	-0.6	Tyr204	H-Pi	4.12
6f	-4.18	-0.5	Gly122	H-donor	4.01

ΔG (Kcal/mole)[a]; The binding free energies

The docking result of the reference compound **NAC** is completely consistent with the mode of action of quinoline/pyrazole derivatives. The 2D diagram showed a crucial binding Arg207 and

Gly122 through quinoline C=O and pyrazole C=N functionality. Moreover, stabilization of the reference NAC within the active site occurred through three strong hydrogen bond interactions with amino acid residue Arg207, Gly122 and Arg64. Docking Results with caspase-3 revealed that most of the tested compounds show good binding with the enzyme and make several interactions comparable to that of the reference NAC. Compounds **6a** and **6b** (Figure 9) exhibited the same interactions with the conserved amino acids as NAC lacked only one H-bonding interaction with Arg64, however, compound **6d** possess greater interaction than NAC to interact with the same amino acids with additional H-Pi bond with Trp206. On the other hand, compounds **6c** and **6e** (Figure 9) dismissed hydrogen binding interactions with the amino acid residue Arg207, Gly122. Compound **6f** kept only hydrogen bond interaction with Gly122 (Figure 9).

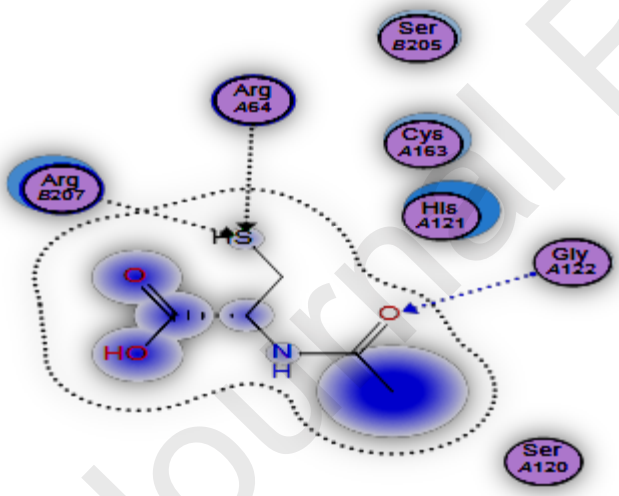

NAC

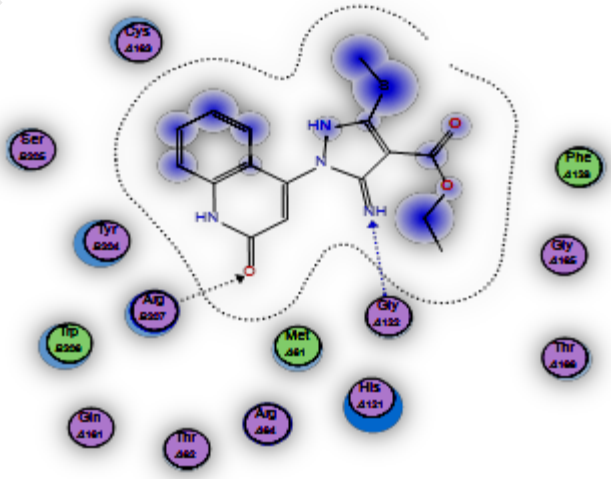

6a

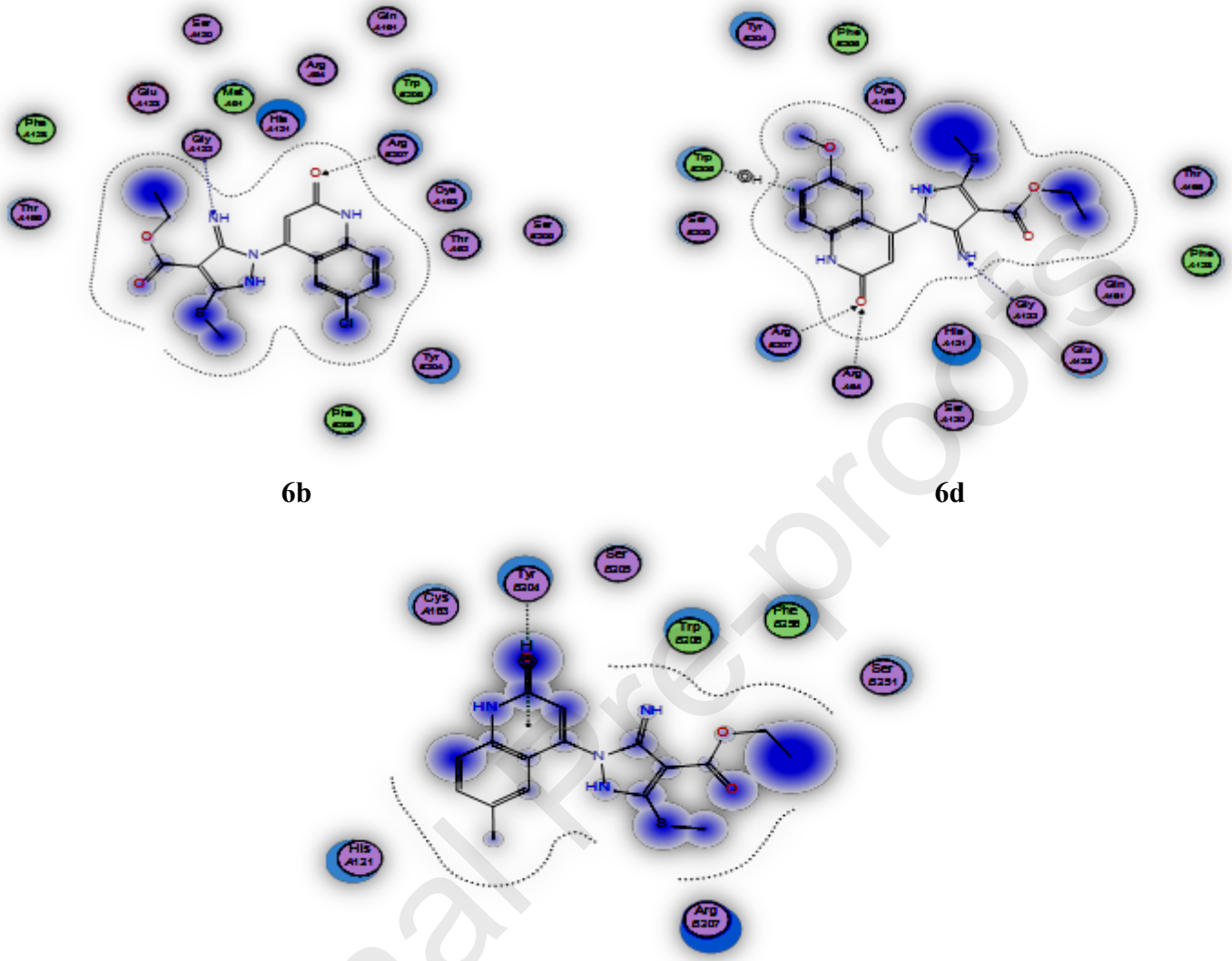

6b **6d**

6e

Figure 9. 2D diagrams illustrate the binding modes of the reference **NAC**, **6a, 6b, 6d** and **6e** interacted with the active site of caspase-3

3. Conclusions

New quinoline-2-one/ pyrazole derivatives **6a-6f** were prepared and characterized by different spectroscopic techniques. It is worth to mention that the tested compounds **6a**, **6c** and **6f** showed more potent activity toward antioxidant and anti-inflammatory biomarkers than quinoline-2-one-/pyrazole derivatives **6d** and **6e**. Histopathological examination for the colonic specimens treated with targeted compounds **6a-6f** indicated that compounds **6a** and **6f** revealed apparent normal

colonic cells, however, compound **6e** showed dilated blood vessels with more apoptotic cells if compared with NAC. Moreover, caspase-3 expression was assayed to exhibit that compound **6a**, **6b** and **6d** provide lower expression to an extent than NAC. Molecular docking studies with caspase-3 enzyme showed comparable binding scores and similar binding interactions as that of the reference NAC. that most of the tested compounds show good binding with the enzyme especially for compound **6d** make several interactions better than that of the reference NAC, however, compound **6b** and **6d** showed more favourable interaction than of the other compounds.

In summary, introduction of a substitution at position 6 of quinoline with either electron donating or withdrawing keeps the same anti-apoptotic activity as unsubstituted derivatives or may be decrease activity due to steric effect. Compounds **6a**, **6c**, and **6f** are promising anti-apoptotic agents that are recommended to be further studied.

4. Experimental

4.1. Chemistry

Melting points were determined using open glass capillaries on a Gallenkamp melting point apparatus (Weiss-Gallenkamp, Loughborough, UK), and are uncorrected. The IR spectra were recorded from potassium bromide disks with a FT device, Minia University NMR spectra were measured in DMSO-d_6 on a Bruker AV-400 spectrometer (400 MHz for ^{1}H, 100 MHz for ^{13}C, and 40.55 MHz for ^{15}N); chemical shifts are expressed in δ (ppm), versus internal tetramethylsilane (TMS) = 0 for ^{1}H and ^{13}C, and external liquid ammonia = 0 for ^{15}N. Coupling constants are stated in Hz. Correlations were established using ^{1}H-^{1}H COSY, and ^{1}H-^{13}C and ^{1}H-^{15}N HSQC and HMBC experiments. Mass spectra were recorded on a Finnigan Fab 70 eV, Institute of Organic Chemistry, Karlsruhe University, Karlsruhe, Germany. TLC was performed

on analytical Merck 9385 silica aluminum sheets (Kieselgel 60) with Pf_{254} indicator; TLC's were viewed at λ_{max} = 254 nm. Elemental analyses were carried out at the Microanalytical Center, Cairo University, Egypt.

4.1.1. General procedure describes the formation of compounds 6a-f

A mixture of aromatic amines **4a-d** (1 mmol) and **5** (2 mmol) in absolute EtOH (100 mL) was refluxed for 10-15 h. The reaction was followed up by TLC analysis. The formed precipitate was kept standing up at room temperature for 24 h. The precipitate which was collected by filtration was washed with 200 mL of EtOH and then dried well. The formed product was then recrystallized from stated solvents.

Ethyl 5-amino-3-(methylthio)-1-(2-oxo-1,2-dihydroquinolin-4-yl)-1*H*-pyrazole-4-carboxylate (6a). Colorless crystals (DMF/EtOH), yield: 210 mg (70 %), mp = 250-252 ^{o}C. IR (KBr, cm^{-1}): 3460-3335 (Ar-NH & Ar-NH_2), 2848 (CH_3, str), 1710 (CO-ester). NMR (DMSO-d_6, δ ppm): Table 1. ESI-MS: *m/z*= 345.1023 (M + 1). Anal. Calcd. for $C_{16}H_{16}N_4O_3S$ (344.39): C, 55.80; H, 4.68; N, 16.27. Found: C, 55.70; H, 4.60; N, 16.10.

Ethyl 5-amino-1-(6-chloro-2-oxo-1,2-dihydroquinolin-4-yl)-3-(methylthio)-1*H*-pyrazole-4-carboxylate (6b). Colorless crystals (DMF/MeOH), yield: 225 mg (77 %), mp = 260-262 ^{o}C. IR (KBr, cm^{-1}): 3350-3320 (NH,NH_2), 3000 (Ar-CH), 2980-2880 (Aliph-CH), 1710 (COOEt). ^{1}H NMR (400 MHz, DMSO-d_6, δ ppm): 12.20 (s, 1H, NH), 7.64 (dd, 1H, *J* = 8.8, 2.0 Hz, H-7), 7.43 (d, 1H, *J* = 1.6 Hz, H-5), 7.35 (d, 1H, *J* = 8.8 Hz, H-8), 6.67 (bs, 3H, H-3,6a'), 4.23 (q, 2H, *J* = 7.0 Hz, H-4b'), 2.36 (s, 3H, SCH_3), 1.29 (t, 3H, *J* = 7.0 Hz, CH_3-ester). ^{13}C NMR (100 MHz, DMSO-d_6, δ ppm): 162.9 (C-4a'), 161.43 (C-2), 152.53 (C-5'), 150.37 (C-3'), 143.04 (C-4), 138.35 (C-8a), 131.11 (C-7), 125.92 (C-6), 125.00 (C-5), 123.57 (C-3), 117.62 (C-8), 117.17 (C-4a), 91.84 (C-4'), 59.13 (C-4b'), 14.44 (C-4c'), 12.26 (C-3a'). ^{15}N (NMR, DMSO-d_6, δ ppm):

181.4 (N-1'), 151.3 (N-1), 60.2 (N-6a'). ESI-MS: *m/z*= 379 (M^++1), 378 (M^+, 34). Anal. Calcd. for $C_{16}H_{15}ClN_4O_3S$ (378.83): C, 50.73; H, 3.99; N, 14.79. Found: C, 50.60; H, 4.10; N, 14.60.

Ethyl 5-amino-1-(6-bromo-2-oxo-1,2-dihydroquinolin-4-yl)-3-(methylthio)-1*H*-pyrazole-4-carboxylate (6c). Colorless crystals (DMF/CH_3CN), yield: 255 mg (88 %), mp = 350-352 ^oC. IR (KBr, cm^{-1}): 3350-3310 (NH, NH_2), 3010 (Ar-CH), 2970-2890 (Aliph-CH), 1712 (COOEt). ^1H (400 MHz, DMSO-d_6, δ ppm): 12.20 (s, 1H, NH), 7.75 (dd, 1H, *J* = 8.7, 1.7 Hz, H-7), 7.50 (d, 1H, *J* = 1.5 Hz, H-5), 7.37 (d, 1H, *J* = 8.8 Hz, H-8), 6.67 (bs, 3H), 4.23 (q, 2H, *J* = 7.0 Hz, H-4b'), 2.36 (s, 3H, SCH_3), 1.29 (t, 3H, *J* = 7.0 Hz, CH_3-ester). ^{13}C NMR (100 MHz, DMSO-d_6, δ ppm): 162.88 (C-4a'), 161.41 (C-2), 152.53 (C-5'), 150.36 (C-3'), 142.93 (C-4), 138.66 (C-8a), 133.76 (C-7), 126.60 (C-5), 124.8 (C-6), 121.06 (C-3), 118.05, 117.85 (C-4a,8), 91.84 (C-4'), 59.14 (C-4b'), 14.44 (C-4c'), 12.37 (C-3a'). ^{15}N (NMR, DMSO-d_6, δ ppm): 180.6 (N-1'), 151.7 (N-1), 60.2 (N-6a'). ESI-MS: *m/z* = 423.0128 (M^++1), 423 (M^+, 32). Anal. Calcd. for $C_{16}H_{15}BrN_4O_3S$ (423.29): C, 45.40; H, 3.57; N, 13.24. Found: C, 45.60; H, 3.60; N, 13.30.

Ethyl 5-amino-1-(6-methoxy-2-oxo-1,2-dihydroquinolin-4-yl)-3-(methylthio)-1*H*-pyrazole-4-carboxylate (6d). Colorless crystals (DMF/EtOH), yield: 230 mg (75 %), mp = 300-302 ^oC (decomp). IR (KBr, cm^{-1}): 3340-3310 (NH, NH_2), 3030-3010 (Ar-CH), 2980-2880 (Aliph-CH), 1710 (COOEt). NMR (DMSO-d_6, δ ppm): Table 2. ESI-MS: *m/z* = 375.1126 (M + 1). Anal. Calcd. for $C_{17}H_{18}N_4O_4S$ (374.42): C, 54.53; H, 4.85; N, 14.96. Found: C, 54.70; H, 4.90; N, 14.80.

Ethyl 5-amino-1-(6-methyl-2-oxo-1,2-dihydroquinolin-4-yl)-3-(methylthio)-1*H*-pyrazole-4-carboxylate (6e). Colorless crystals (DMF/H_2O), yield: 222 mg (73 %), mp = 330-332 ^oC. IR (KBr, cm^{-1}): 3330-3312 (NH, NH_2), 3015 (Ar-CH), 2990-2890 (Aliph-CH), 1710 (COOEt). ^1H (400 MHz, DMSO-d_6, δ ppm): 12.00 (s, 1H, NH), 7.41 (dd, 1H, *J* = 8.4 Hz, H-7), 7.32 (d, 1H, *J*

= 8.4 Hz, H-8), 7.13 (bs, 1H, H-5), 6.58 (bs, 2H), 6.55 (s, 1H, H-3), 4.23 (q, 2H, *J* = 7.1 Hz, H-4b'), 2.35 (s, 3H, SCH_3), 2.30 (s, 3H, CH_3), 1.29 (t, 3H, *J* = 7.0 Hz, CH_3-ester). ^{13}C NMR (100 MHz, DMSO-d_6, δ ppm): 163.10 (C-4a'), 161.50 (C-2), 152.34 (C-5'), 149.82 (C-3'), 144.02 (C-4), 137.64 (C-8a), 132.45 (C-7), 131.00 (C-6), 123.82 (C-5), 120.20 (C-3), 116.43 (C-4a), 115.56 (C-8), 91.69 (C-4'), 59.07 (C-4b'), 20.59 (Ar-CH_3), 14.46 (C-4c'), 12.36 (C-3a'). ^{15}N (NMR, DMSO-d_6, δ ppm): 180.5 (N-1'), 150.8 (N-1), 59.8 (N-6a'). ESI-MS: *m/z*= 359.1176 (M + 1). Anal. Calcd. for $C_{17}H_{18}N_4O_3S$ (358.42): C, 56.97; H, 5.06; N, 15.63. Found: C, 57.10; H, 5.20; N, 15.70.

Ethyl 5-amino-1-(1-methyl-2-oxo-1,2-dihydroquinolin-4-yl)-3-(methylthio)-1*H*-pyrazole-4-carboxylate (6f). Pale yellow crystals (DMF/EtOH), yield: 218 mg (72%), mp = 310-312 °C (decomp). IR (KBr, cm^{-1}): 3330-3310 (NH, NH_2), 3040-3020 (Ar-CH), 2970-2860 (Aliph-CH), 1708 (COOEt). NMR (DMSO-d_6, δ ppm): Table 3. ESI-MS: *m/z*= 359.1176 (M +1), 313.1 (M^+-SCH_3). Anal. Calcd. for $C_{17}H_{18}N_4O_3S$ (358.42): C, 56.97; H, 5.06; N, 15.63. Found: C, 57.08; H, 5.12; N, 15.72.

4.2. Biological activity

4.2.1. Material and methods

1. The 200 mg rats were chosen and grouped for 7 groups (each contains 5 rats (n=5) as following: G1 = Sham, G2 = Model (I/R), G3 = NAC, G4-9 of compounds **6a-f**
2. The compounds were injected intraperitoneally for 1 h before anesthetization by 0.25 ml urethane and surgery.
3. The rats were operated to close superior mesenteric vein by clamps for 0.5 h (ischemia) and reopened (reperfusion) for 0.5 h.

4. After that, blood samples were collected from the ventricular of the heart centrifuged (centrifuge Jantezki, T30, Germany), at 5000 rpm for 10 min for serum collection. Sera were separated and kept in refrigerator at -80°C until assessment of various parameters.
5. At the end, the rats were killed to obtain colon for biological and histological studies.
6. Intestinal tissue of each rat was rapidly dissected, left to dry on filter paper, weighed and prepared for histopathological and immunohistochemical examinations or stored at -80°C for further measurements.
7. 200 Mg of intestine was homogenized in 2 ml of phosphate buffer solution (prepared by dissolving 8.01 g NaCl, 0.20 g KCl, 1.78 g Na_2HPO_4, $2H_2O$ and 0.27 g KH_2PO_4 in 1 liter of distilled water and pH = 7.4) using homogenizer (Tri-R Stir-R homogenizer, Tri-R Instruments, Inc., Rockville Centre, NY).

4.2.2. Determination of lipid peroxides in the form of Malondialdehyde (MDA) in the intestine

MDA, a reactive aldehyde that is a measure of lipid peroxidation, bone marrow cardiac contents of MDA were determined using the thiobarbituric acid method described by Buege and Aust (1978) [41], which measures the thiobarbituric acid reactive substances concentration, sometimes referred to as MDA concentration.

Principle

This method measures the intestinal MDA level which is the breakdown product of tissue lipid peroxides.

Procedures

- To a 0.5 mL of 10 % homogenate of the tissue sample, 0.5 mL of distilled water was added.
- The reagent was freshly prepared (26 mmol/L thiobarbituric acid, 0.92 mol/L trichloroacetic acid in 0.25 mol/L HCl) and 2 mL were added to each tube.

- The mixture was heated in a boiling water bath for 15 min.
- After cooling, the supernatant was removed by centrifugation at 5000 rpm for 10 min.
- The absorbance of the sample was determined at 535 nm against a blank using Beckmann DU-64 spectrophotometer **(**Phoenix Equipment Inc, New York).

1,1,3,3–Tetramethoxypropane was used as an external standard to prepare standard concentrations of MDA (1,2,4,6,8 and 10 nmol/mL) and the procedure was repeated to prepare a standard curve using 1,1,3,3–tetramethoxypropane instead of colonic homogenates [41]. From this curve, the MDA concentration in the unknown sample was extrapolated from the corresponding absorbance using the regression line from the standard curve then multiplied in tissue and expressed as nmol/g tissue.

Standard curve of MDA

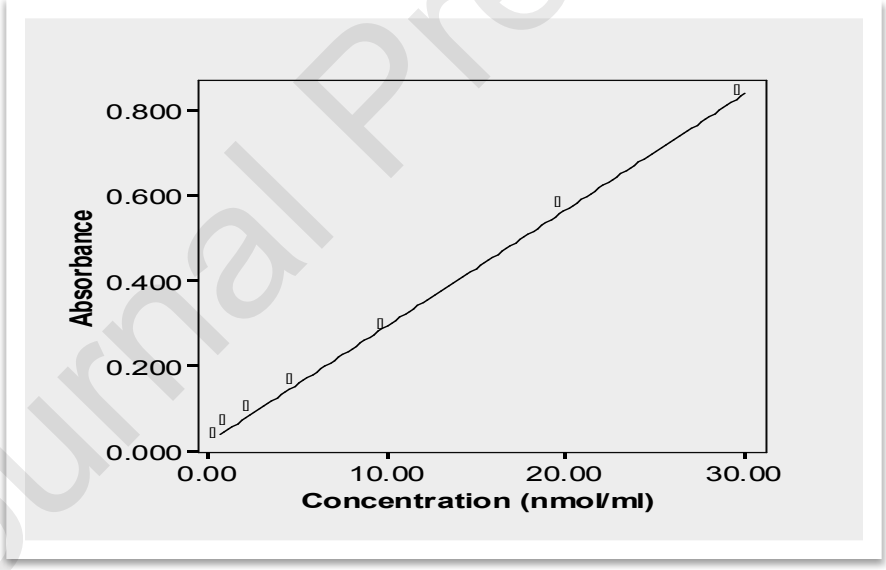

4.2.3. Determination of superoxide dismutase (SOD) in the intestine

SOD activity was determined according to the previously described method.

Principle

The method is based on the fact that the autoxidation of pyrogallol is inhibited by SOD. One unit of SOD is generally defined as the amount of enzyme that inhibits the autoxidation of pyrogallol by 50%.

The activity of SOD was measured by Marklund's method [42] with a slight modification. This method depends on inhibition of the pyrogallol autooxidation by SOD. Calculation of the percentage of inhibition for the samples was done by the aid of running a control with no sample under the same conditions. SOD activity was expressed in units; where the unit equals the amount of the enzyme that inhibited 50% of pyrogallol autoxidation. F is the weight of tissue per 1 ml of homogenate, which is equivalent to 0.1 g/ml homogenate.

4.2.4. Determination of reduced glutathione

Reduced glutathione (GSH) was measured using colorimetric kit according to the method described by Beutler et al. (1963)[43].

4.3. Histological examination

Colonic specimens were obtained from each group and fixed in 10% formol saline for 24 h. Paraffin blocks were carried on and 5-µm thick sections were subjected to H&E, Perly's stain[44].

4.4. Caspase inhibition assay method

4.4.1. Caco-2 cells treatment

Caco-2 cells were purchased from vacsera, Egypt. Cells were plated in 12 well plates in 10% FBS- RPMI medium at a density of 1×10^5 cells/well. Cells were given 24 h to attach, then were stimulated with either LPS (1 ug/mL, InvivoGen, Cat no. # tlrl-kit1hw) or PBS as a control, and incubated at 37°C plus 5% CO_2. After 6 h, LPS stimulated cells were treated with M-42, M-43, M-44, M-45, M-46, and M-47 (10 uM). Some LPS stimulated cells left without treatment. Then

all cells were incubated at 37°C plus 5% CO_2. After 24 h, the cells were washed with PBS then harvested for RNA extraction.

4.4.2. Real-time PCR

RNA was extracted using the RNeasy kit (Qiagen) according to the manufacturer's instructions. Nano Drop was used for quantification and checking purity of RNA (260/280 ~1.8). cDNA was prepared using High- Capacity Reverse Transcriptase kit (Applied Biosystems, Foster City, CA, USA) in a VeritiTM 96-well Thermal Cycler (Applied Biosystems, Foster City, CA, USA). Gene expression for Caspase-3 was measured by Real-Time quantitative PCR (qPCR) which was performed using StepOnePlus with SYBR Green and specific primers (see Table 9 for primer sequence). mRNA levels were normalized to GAPDH, which produced comparable results. Real-time qPCR reaction conditions comprised initial denaturation at 95 °C for 10 min, followed by 40 cycles of 95 °C for 15 sec and 60 °C for 60 sec. A melt curve analysis was performed at the end of each run of the SYBR Green protocol to confirm the generation of specific PCR products. The fold change of each gene was calculated using the Delta-delta threshold (ΔCt) data analysis method.

Statistical methods are detailed in the supplementary methods. All tests were two-tailed and *P* values <0.05 were considered significant.

Table 9. StepOnePlus with SYBR Green and specific primers of PCR

Gene name	Forward Primer	Reverse Primer
Human Caspase-3	5′-TTCAGAGGGGATCGTTGTAGAAGTC-3′	5′-CAAGCTTGTCGGCATACTGTTTCAG-3′
Human GAPDH	5′-AGCCACATCGCTCAGACAC-3′	5′- GCCCAATACGACCAAATCC-3′

4.5. Docking studies

Docking simulation study is performed using Molecular Operating Environment (MOE®) version 2014.09, Chemical Computing Group Inc., Montreal, Canada. The

computational software operated under "Windows XP" installed on an Intel Pentium IV PC with a 1.6 GHz processor and 512 MB memory. The target compounds were constructed into a 3D model using the builder interface of the MOE program. After checking their structures and the formal charges on atoms by 2D depiction, the following steps were carried out:

- All conformers were subjected to energy minimization, all the minimizations were performed with MOE until a RMSD gradient of 0.01 Kcal/mole and RMS (Root Mean Square) distance of 0.1 Å with MMFF94X force-field and the partial charges were automatically calculated.
- The obtained database was then saved as Molecular Data Base (MDB) file to be used in the docking calculations.

Optimization of the target

The X-ray crystallographic structure of the target Topoisomerase II enzyme (PDB: 6CKZ) obtained from Protein data bank. The compounds were docked on the active site the target enzyme.

The enzyme was prepared for docking studies by:

- The co-crystallized ligand was deleted.
- Hydrogen atoms were added to the system with their standard geometry.
- The atoms connection and type were checked for any errors with automatic correction.
- Selection of the receptor and its atoms potential were fixed.

Docking of the target molecules to caspase-3 enzyme active site

Docking of the target compounds was done using MOE-Dock software. The following methodology was generally applied:

- The enzyme active site file was loaded, and the Dock tool was initiated. The program specifications were adjusted to:

- Dummy atoms as the docking site.

- Triangle matcher as the placement methodology to be used.

- London δG as Scoring methodology to be used and was adjusted to its default values.

- The MDB file of the ligand to be docked was loaded and Dock calculations were run automatically.
- The obtained poses were studied, and the poses showed best ligand-enzyme interactions were selected and stored for energy calculations.

5. Acknowledgment

The authors thank the Deutsche Forschungsgemeinschaft (DFG) for their financial support of the accommodation of Prof Aly during his staying at the Karlsruhe Institute of Technology, Karlsruhe, Germany during the period of July/August 2019.

6. Conflict of Interest

No financial or commercial conflicts of interest were declared by all authors

7. References

[1] N.N. Danial, S.J. Korsmeyer, Cell death: critical control points, Cell 116(2) (2004) 205-19.

[2] S. Bulut, B.H. Özdemir, Apoptosis and expression of caspase-3 in cyclosporin-induced gingival overgrowth, J. Periodontology 78(12) (2007) 2364-2368.

[3] V. Sagulenko, K.E. Lawlor, J.E. Vince, New insights into the regulation of innate immunity by caspase-8. Bio. Med. Central, 2016.

[4] X. Pu, S.J. Storr, Y. Zhang, E.A. Rakha, A.R. Green, I.O. Ellis, S.G. Martin, Caspase-3 and caspase-8 expression in breast cancer: caspase-3 is associated with survival, Apoptosis 22(3) (2017) 357-368.

[5] C.-C. Wang, H. Li, M. Zhang, X.-L. Li, L.-T. Yue, P. Zhang, Y. Zhao, S. Wang, R.-N. Duan, Y.-B. Li, Caspase-1 inhibitor ameliorates experimental autoimmune myasthenia gravis by innate dendric cell IL-1-IL-17 pathway, J.Neuroinflamm. 12(1) (2015) 118.

[6] N.E. Akpan, The intrinsic caspase death pathway in stroke neurodegeneration, Columbia University2013.

[7] X.-J. Wang, Q. Cao, Y. Zhang, X.-D. Su, Activation and regulation of caspase-6 and its role in neurodegenerative diseases, Ann. Rev. Pharm. & Tox. 55 (2015) 553-572.

[8] P.K. Singh, A. Kumar, Mitochondria mediates caspase-dependent and independent retinal cell death in Staphylococcus aureus endophthalmitis, Cell Death Discovery 2 (2016) 16034.

[9] C. Sun, H. Liu, J. Guo, Y. Yu, D. Yang, F. He, Z. Du, MicroRNA-98 negatively regulates myocardial infarction-induced apoptosis by down-regulating Fas and caspase-3, Scientific Reports 7(1) (2017) 7460.

[10] B.L. Woolbright, W.-X. Ding, H. Jaeschke, Caspase inhibitors for the treatment of liver disease: friend or foe?, Expert Rev Gastroenterol Hepatol 11(5) (2017) 397-399.

[11] M. Aziz, A. Jacob, P. Wang, Revisiting caspases in sepsis, Cell Death Dis 5(11) (2014) e1526-e1526.

[12] H.S. Hwang, H.A. Kim, Chondrocyte Apoptosis in the Pathogenesis of Osteoarthritis, Int J Mol Sci 16(11) (2015) 26035-26054.

[13] I.E. Malysheva, L.V. Topchieva, O.Y. Barysheva, I.V. Kurbatova, O.A. Vasykova, N.N. Vezikova, I.M. Marusenko, N.N. Nemova, The level of cytokines and expression of caspase genes in rheumatoid arthritis. Doklady Biochem. & Biophy. 468(1) (2016) 226-228.

[14] X. Qi, P. Gurung, R.K.S. Malireddi, P.W.F. Karmaus, D. Sharma, P. Vogel, H. Chi, D.R. Green, T.D. Kanneganti, Critical role of caspase-8-mediated IL-1 signaling in promoting Th2 responses during asthma pathogenesis, Mucosal Immunol 10(1) (2017) 128-138.

[15] E.-S.M.N. Abdelhafez, S.M.N.A. Ali, M.R.E. Hassan, A.M. Abdel-Hakem, Apoptotic Inhibitors as Therapeutic Targets for Cell Survival, Cytotoxicity, IntechOpen2019. Doi.10.5772/intechopen.85465

[16] A. Onder, M. Kapan, M. Gumus, H. Yuksel, A. Boyuk, H. Alp, M.K. Basarili, U. Firat, The protective effects of curcumin on intestine and remote organs against mesenteric ischemia/reperfusion injury. Turk. J. Gastroenterology. 23(2) (2012) 141-7.

[17] T. Cui, M. Miksa, R. Wu, H. Komura, M. Zhou, W. Dong, Z. Wang, S. Higuchi, W. Chaung, S.A. Blau, C.P. Marini, T.S. Ravikumar, P. Wang, Milk fat globule epidermal growth factor 8 attenuates acute lung injury in mice after intestinal ischemia and reperfusion, Am. J. Resp. & Crit. Care Med. 181(3) (2010) 238-46.

[18] H.K. Eltzschig, T. Eckle, Ischemia and reperfusion--from mechanism to translation, Nature Med. 17(11) (2011) 1391-401.

[19] M. Kojima, R. Iwakiri, B. Wu, T. Fujise, K. Watanabe, T. Lin, S. Amemori, H. Sakata, R. Shimoda, T. Oguzu, A. Ootani, S. Tsunada, K. Fujimoto, Effects of antioxidative agents on apoptosis induced by ischaemia-reperfusion in rat intestinal mucosa, Alimentary pharmacology & therapeutics 18 Suppl 1 (2003) 139-45.

[20] N. Tomatsuri, N. Yoshida, T. Takagi, K. Katada, Y. Isozaki, E. Imamoto, K. Uchiyama, S. Kokura, H. Ichikawa, Y. Naito, T. Okanoue, T. Yoshikawa, Edaravone, a newly developed radical scavenger, protects against ischemia-reperfusion injury of the small intestine in rats, Intern. J. Mol. Med. 13(1) (2004) 105-9.

[21] M.H. Schoenberg, B.B. Fredholm, U. Haglund, H. Jung, D. Sellin, M. Younes, F.W. Schildberg, Studies On The Oxygen Radical Mechanism Involved In The Small Intestinal Reperfusion Damage, Acta Physiologica Scand. 124(4) (1985) 581-589.

[22] L.M. Havran, D.C. Chong, W.E. Childers, P.J. Dollings, A. Dietrich, B.L. Harrison, V. Marathias, G. Tawa, A. Aulabaugh, R. Cowling, B. Kapoor, W. Xu, L. Mosyak, F. Moy, W.T. Hum, A. Wood, A.J. Robichaud, 3,4-Dihydropyrimido(1,2-a)indol-10(2*H*)-ones as potent non-peptidic inhibitors of caspase-3, Bioorg. & Med. Chem. 17(22) (2009) 7755-68.

[23] E.M. El-Sheref, A.A. Aly, A.-F.E. Mourad, A.B. Brown, S. Bräse, M.E. Bakheet, Synthesis of pyrano[3,2-*c*]quinoline-4-carboxylates and 2-(4-oxo-1,4-dihydroquinolin-3-yl)fumarates, Chem. Pap.72(1) (2018) 181-190.

[24] A.A. Aly, E.M. El-Sheref, A.-F.E. Mourad, A.B. Brown, S. Bräse, M.E. Bakheet, M. Nieger, Synthesis of spiro[indoline-3,4′-pyrano[3,2-*c*]quinolone]-3′-carbonitriles, Monatsh.Chem. 149(3) (2018) 635-644.

[25] A.A. Aly, E.M. El-Sheref, A.-F.E. Mourad, M.E.M. Bakheet, S. Bräse, M. Nieger. One-pot synthesis of 2,3-bis-(4-hydroxy-2-oxo-1,2-dihydroquinolin-3-yl)succinates and aryl-methylene-bis-3,3′-quinoline-2-ones. Chem. Pap. 73(2019):27–37.

[26] A.A. Aly, M. Ramadan, A.A. M. El-Reedy. Reactions of 4-Hydroxyquinolin-2(1*H*)-ones with Acenaphthoquinone: Synthesis of New 1,2-Dihydroacenaphthylene-spiro-tetrakis-(4-hydroxyquinolin-2(1*H*)-ones). J. Heterocycl. Chem. 56 (2019):642-645.

[27] A.A. Aly, E.M. El-Sheref, M.E.M. Bakheet, M.A.E. Mourad, S. Bräse, M.A.A. Ibrahim, M. Nieger, B.K. Garvalov, K.N. Dalby, T.S. Kaoud. Design, synthesis and biological evaluation of fused naphthofuro[3,2-*c*]quinoline-6,7,12-triones and pyrano[3,2-*c*]quinoline-6,7,8,13-tetraones derivatives as ERK inhibitors with efficacy in BRAF-mutant melanoma. Biorg. Chem. 82 (2019) 290–305.

[28] A.A. Aly, E.M. El-Sheref, M.E.M. Bakheet, M.A.E.Mourad, A.B. Brown, S. Bräse, M. Nieger, M.A.A. Ibrahim. Synthesis of novel 1,2-bis-quinolinyl-1,4-naphthoquinones: ERK2 inhibition, cytotoxicity and molecular docking studies. 81 (2018):700-712.

[29] A.A. Aly, E.M. El-Sheref, A-F.E. Mourad, M.E.M. Bakheet, S. Bräse. 4-Hydroxy-2-quinolones: syntheses, reactions and fused heterocycles. Mol. Diver. 2019 (in press). https://doi.org/10.1007/s11030-019-09952-5

[30] M.A.I. Elbastawesy, A.A. Aly, M. Ramadan, Y.A.M.M. Elshaier, B.G.M. Youssif, A.A. Brown, G.El-D.A. Novel Pyrazoloquinolin-2-ones: Design, synthesis, docking studies, and biological evaluation as antiproliferative EGFR-TK inhibitors. Biorg Chem. 90 (2019) 103045-103061

[31] M. Abass, Chemistry of substituted quinolinones. part II Synthesis of novel 4-pyrazolylquinolinone derivatives, Synthetic Communications, 30 (2000) 2735-2757.

[32] M.M. Ismail, M. Abass, M.M. Hassan, Chemistry of substituted quinolinones. Part VI. Synthesis and nucleophilic reactions of 4-chloro-8-methylquinolin-2(1*H*)-one and its thione analogue, Molecules, 5 (2000) 1224-1239.

[33] M. Ismail, M. Abdel-Megid, M. Hassan, Some reactions of 2-and 4-substituted 8-methylquinolin-2(1*H*)-ones and their thio analogues, Chemical papers-slovak academy of Sciences. 58 (2004) 117-125.

[34] F.-X. Zhang, M.-l. Chen, B. Yang, H.-w. Chen, W.-z. Ju, J. Wang, K.-j. Cao, [The anti-apoptotic effects of *N*-acetylcysteine in neonatal rat cardiomyocytes underwent hypoxia-reoxygenation injury], Zhonghua Xin Xue Guan Bing Za Zhi 38(5) (2010) 445-449.

[35] D. Derin, H.O. Soydinc, N. Guney, F. Tas, H. Camlica, D. Duranyildiz, V. Yasasever, E. Topuz, Serum levels of apoptosis biomarkers, survivin and TNF-alpha in nonsmall cell lung cancer. Lung Cancer (Amsterdam, Netherlands) 59(2) (2008) 240-5.

[36] A.A.-M. El-Badry, Serum Malondialdehyde Levels as a Biomarker of Cellular Injury In Human Fascioliasis, Journal of Taibah University Medical Sciences 1(1, Supplement C) (2006) 57-64.

[37] D. Gershov, S. Kim, N. Brot, K.B. Elkon, C-Reactive protein binds to apoptotic cells, protects the cells from assembly of the terminal complement components, and sustains an antiinflammatory innate immune response: implications for systemic autoimmunity. J. Exp. Med. 192(9) (2000) 1353-64.

[38] I. Petrache, T.R. Medler, A.T. Richter, K. Kamocki, U. Chukwueke, L. Zhen, Y. Gu, J. Adamowicz, K.S. Schweitzer, W.C. Hubbard, E.V. Berdyshev, G. Lungarella, R.M. Tuder, Superoxide dismutase protects against apoptosis and alveolar enlargement induced by ceramide, American journal of physiology. Lung cellular and molecular physiology 295(1) (2008) L44-53.

[39] G.M. Enns, T.M. Cowan, Glutathione as a Redox Biomarker in Mitochondrial Disease-Implications for Therapy, J. Clin. Med.6(5) (2017).

[40] E. Crosas-Molist, I. Fabregat, Role of NADPH oxidases in the redox biology of liver fibrosis, Redox Biol 6 (2015) 106-111.

[41] J.A. Buege, S.D. Aust, Microsomal lipid peroxidation, Methods in Enzymology 52 (1978) 302-10.

[42] S. Marklund, G. Marklund, Involvement of the superoxide anion radical in the autoxidation of pyrogallol and a convenient assay for superoxide dismutase, Eur. J. Biochem. 47(3) (1974) 469-74.

[43] E. Beutler, O. Duron, B.M. Kelly, Improved method for the determination of blood glutathione, J. Lab. & Clin. Med. 61 (1963) 882-8.

[44] J.D. Bancroft, M. Gamble, Theory and practice of histological techniques, Churchill Livingstone, London, 2008.

Novel quinoline-2-one/pyrazole Derivatives; Design, Synthesis, Molecular Docking, Anti-apoptotic Evaluation, and Caspase-3 Inhibition Assay

Ashraf A. Aly, Samia M. Sayed, El-Shimaa M. N. Abdelhafez, Sara Mohamed Naguib Abdelhafez, Walaa Yehia Abdelzaher, Mohamed A. Raslan, Amira E. Ahmed, Khaled Thabet, Ahmed A. M. El-Reedy, Alan B. Brown and Stefan Bräse

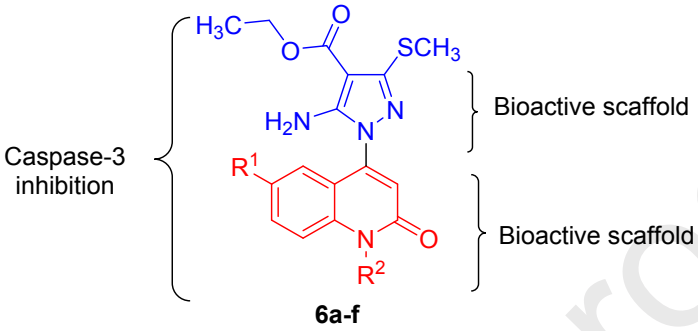

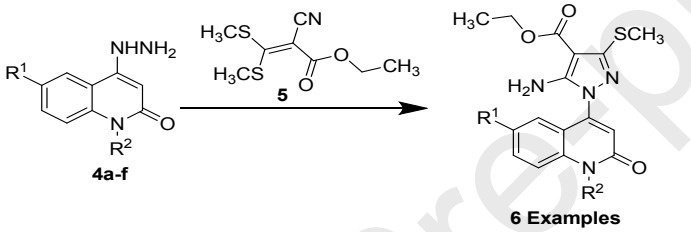

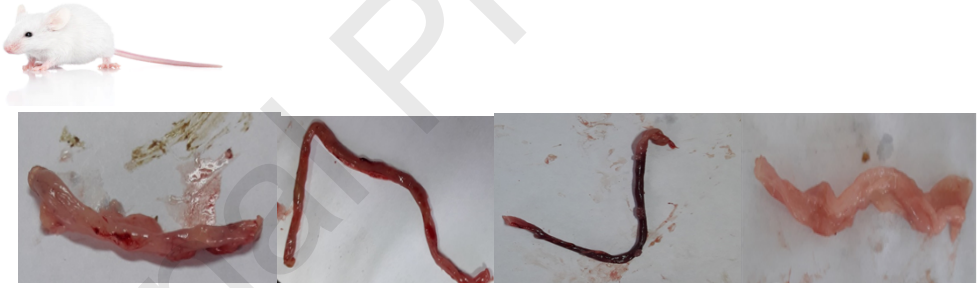

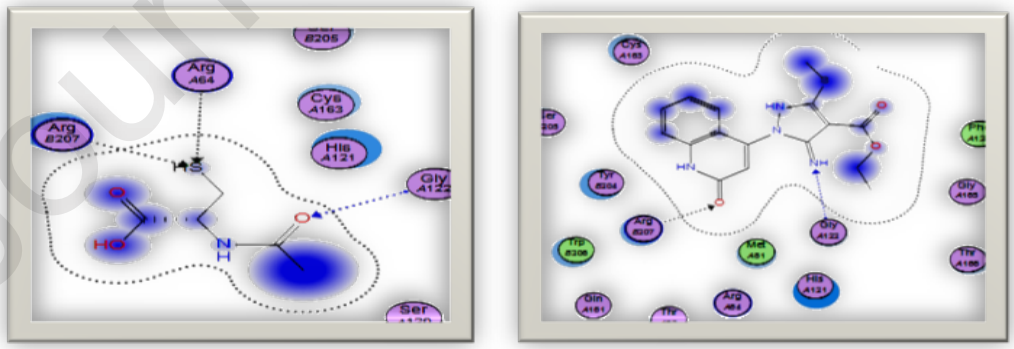

Highlights

1- Synthesis of new pyrazolo-quinoline-2-ones.
2- NMR spectra as effective tool to elucidate the given structure.
3- Some compounds showed significant improvement for oxidative stress parameters MDA, SOD, GSH and NOx in comparison with model group and greater than NAC
4- Colonic histopathological investigation was performed on all targeted compounds.
5- H&E sections of some compounds revealed apparent normal colonic cells compared with NAC.
6- Docking studies with caspase-3 revealed that most of the tested compounds show good binding with the enzyme.